

Journal of Intelligent Material Systems and Structures

<http://jim.sagepub.com/>

On the fundamental and superharmonic effects in bistable energy harvesting

RL Harne and KW Wang

Journal of Intelligent Material Systems and Structures 2014 25: 937 originally published online 3 September 2013

DOI: 10.1177/1045389X13502856

The online version of this article can be found at:

<http://jim.sagepub.com/content/25/8/937>

Published by:



<http://www.sagepublications.com>

Additional services and information for *Journal of Intelligent Material Systems and Structures* can be found at:

Email Alerts: <http://jim.sagepub.com/cgi/alerts>

Subscriptions: <http://jim.sagepub.com/subscriptions>

Reprints: <http://www.sagepub.com/journalsReprints.nav>

Permissions: <http://www.sagepub.com/journalsPermissions.nav>

Citations: <http://jim.sagepub.com/content/25/8/937.refs.html>


>> [Version of Record](#) - Apr 22, 2014

[OnlineFirst Version of Record](#) - Sep 3, 2013

[What is This?](#)

On the fundamental and superharmonic effects in bistable energy harvesting

RL Harne and KW Wang

Journal of Intelligent Material Systems and Structures
2014, Vol. 25(8) 937–950
© The Author(s) 2013
Reprints and permissions:
sagepub.co.uk/journalsPermissions.nav
DOI: 10.1177/1045389X13502856
jim.sagepub.com


Abstract

Superharmonic dynamics are characteristic of many nonlinear systems undergoing high levels of excitation. However, what constitutes high levels is relative to the system under study. For instance, bistable oscillators may have very low linearized natural frequency which often becomes a normalization parameter for excitation in analysis. Thus, high excitation levels may be a common operating condition for bistable oscillators. Recent experimental energy harvesting investigations using bistable devices (referred to as bistable energy harvesting) have observed superharmonic spectral and phenomenological effects yielding superior electrical power relative to that achieved by the fundamental harmonic. To provide a thorough analytical framework to probe the collective fundamental and superharmonic effects on bistable energy harvester power harvesting performance, this article employs the method of harmonic balance to predict the resulting electrodynamic responses applicable to piezoelectric and electromagnetic coupling configurations. The analytical results exemplify the relative ease by which significant superharmonic effects are activated and dominate spectral characteristics, potentially to greatly benefit energy harvesting. The conclusions are corroborated by trends observed in previously published investigations and are validated by present numerical results and experimental findings. This study provides new insights and suggests that careful understanding of excitation characteristics is needed for optimum bistable energy harvesting in practice.

Keywords

Superharmonics, bistable energy harvester, electromagnetic, piezoelectric

Introduction

The ultimate goal of vibration-based energy harvesting is to convert as much as possible the ambient environmental vibration into electrical energy to reduce reliance on wired or disposable power sources. This is oftentimes achieved using devices of the form of electrically damped mass–spring oscillators, designed so as to resonate at the frequency most dominant in the environment vibration spectrum (Stephen, 2006; Williams and Yates, 1996). This design approach is justified if the ambient vibration is narrowband in frequency and remains stationary over long periods of time. However, a typical ambient vibration spectrum is often the result of stochastic excitation that becomes low-pass filtered as a result of the environment or host structure itself (Daqaq, 2011). This is the characteristic of many engineering structures, for example, bridges or buildings, which exhibit low-frequency modal vibration but are driven by decidedly white noise sources such as automotive tire forces or cross-wind (Rao, 1984). Likewise, ocean waves are excited by the stochastic nature of

wind but are effectively low-pass filtered such that ocean wave energy is heavily concentrated at frequencies below 1 Hz (Falnes, 2002).

While great headway has been made in linear energy harvesting research, the above-mentioned realistic vibration sources pose difficulty in designing linear harvesters suitable for such a distribution of the available vibration energy. Thus, a variety of nonlinearities have been studied to exploit their resulting dynamics for improved broadband performance (Tang et al., 2010; Zhu et al., 2010). Of these, bistable harvesters have received much attention due to their capability of achieving high velocity and displacement per cycle as the devices snap through from one stable state to the

Department of Mechanical Engineering, University of Michigan, Ann Arbor, MI, USA

Corresponding author:

RL Harne, Department of Mechanical Engineering, University of Michigan, Ann Arbor, MI 48109-2125, USA.
Email: rharne@umich.edu

next (Harne and Wang, 2013). Conveniently, snap-through may be excited regardless of the form or frequency of input excitation (i.e. it is not a resonant effect), potentially making bistable harvesters more beneficial in realistic vibration environments (Daqaq, 2011). Since steady-state electrical output is dependent on the response amplitude of the harvester inertial mass, the snap-through effect is propitious for energy harvesting. As a result, recent analytical and experimental investigations in bistable energy harvesting have rapidly multiplied (Betts et al., 2012; Erturk et al., 2009; Ferrari et al., 2010; Harne et al., 2013; Harne and Wang, 2013; Kim and Kim, 2013; Mann and Owens, 2010).

Analysis of bistable energy harvesters was initially conducted with numerical integration case studies (Erturk et al., 2009; Mann and Owens, 2010) which provided insight, but lack the ability to draw generalized conclusions regarding performance expectations or design guidelines. In particular, analytical methods which yield information in the frequency domain may help to better understand the characteristics of bistable harvesters operating in complex spectral environments. Therefore, a number of researchers have recently utilized analytical techniques such as the method of multiple scales (MMS) (Karami and Inman, 2011), stochastic differential equation solution (Daqaq, 2011, 2012), and Melnikov theory (Stanton et al., 2012a) to provide more rigorous assessment of bistable harvesters relative to other designs such as monostable Duffing or a baseline linear harvester.

Some works have also used the method of harmonic balance (Mann et al., 2012; Stanton et al., 2012b). Like MMS, this method truncates an exact series expansion solution to a finite number of terms so as to provide for tractable equations governing system responses. Yet, unlike MMS and other perturbation techniques, the method of harmonic balance does not necessitate assumption of small nonlinear terms (i.e. no perturbation parameter requirement) and is therefore better suited to modeling the strongly nonlinear dynamics of bistable systems (Feeny and Yuan, 2001; Tweten and Mann, 2013; Yuan and Feeny, 1998). In their original demonstration of the dynamics of a postbuckled beam, Tseng and Dugundji (1971) demonstrated the quantitative and qualitative accuracy of the harmonic balance method in fundamentally characterizing intra- and interwell responses. The method uses the Fourier series expansion

$$r(t) = c(t) + \sum_{k=1}^N a_k(t) \sin(k\omega t) + b_k(t) \cos(k\omega t) \quad (1)$$

where the number of terms N determines the fidelity of the modeled result. An exact solution, $N = \infty$, is computationally infeasible, and in general the relative

importance of additional harmonics declines substantially after the first few, depending on the nonlinearities involved. Additional terms of order k represent other spectral lines at frequencies $k\omega$ induced in consequence to excitation at frequency ω . Stanton et al. (2012b) and Mann et al. (2012) used a one-term expansion which provided an assessment of the fundamental dynamics of the bistable harvester.

In recent works by Masana and Daqaq (2011, 2012), it was shown by numerical and experimental results that the superharmonic responses of bistable energy harvesters—that is, dynamics occurring at integer fractions of the fundamental frequency—may become more substantial as the relative excitation levels increase. The phenomena were found to potentially yield more substantial electrical output than fundamental harmonic responses. Since what is defined as relative excitation amplitude is normalized to the linear stiffness of the harvester (equivalently, the linear natural frequency), which may be very small for bistable devices, it is prudent to consider additional harmonic effects in a bistable energy harvesting analysis. Indeed, the amplitude of excitation employed by Masana and Daqaq (2012) that was found to induce significant superharmonic effects was only 5.5 m/s^2 (0.56 g) which is an average acceleration level compared to other bistable energy harvesting research employing similarly sized devices (Erturk et al., 2009; Ferrari et al., 2010; Mann and Owens, 2010).

Given the observed sensitivity of inducing prominent superharmonic spectral content and phenomena for bistable devices, it is beneficial to conduct a thorough analytical investigation of a bistable energy-harvesting device accounting for superharmonic effects that provides insight into the onset and range of influence of these key dynamics. This research seeks to provide such an analytical framework by extending the harmonic balance method to include components of the third harmonic and validates the findings via experiments and simulations. The focus is on the interwell, snap-through responses and the spectral content of first and third harmonics induced in consequence to various excitation frequencies and levels, that is, excitation provided at frequency ω , and responses induced at ω and 3ω . Since the nonlinear stiffness of bistable energy harvesters is often modeled as cubic, only odd harmonics are induced as a result of interwell response (Malatkar and Nayfeh, 2007; Szemplińska-Stupnicka, 1968), justifying the focus of this work. With this framework, we can provide predictions and insights on prevalent superharmonic phenomena that are inherently absent in fundamental harmonic balance investigations and which play important roles in tailoring energy harvesting performance for bistable systems.

This article is organized as follows. The following section presents the model of a bistable energy-harvesting device having piezoelectric or electromagnetic conversion

mechanisms, derives amplitude response equations using the harmonic balance method, and describes the procedure undertaken to solve the coupled nonlinear equations. We then compare the results of the present method with the one-term harmonic balance solution previously used in the literature that exemplifies the substantial differences even for relatively low excitation levels. Dynamic response predictions for higher excitation levels are presented, where it is found that superharmonic response dramatically affects energy harvesting. Because of the redistribution of vibrational energy over the spectrum, we then focus on the superharmonic bandwidth to determine the range of excitation characteristics suitable for enhanced superharmonic energy harvesting. In addition to previously published experimental studies which validate the present analytical evaluation, we present new supporting experimental and numerical evidence to validate the predictions. Concluding remarks are then provided to summarize key findings.

Bistable energy harvester modeling

Governing equations

Following nondimensionalization, the governing equations for piezoelectrically or electromagnetically coupled bistable energy harvesters connected to harvesting circuit load resistances are identical, with the exception of the coupling coefficient interpretation. Therefore, for a more extensible application of the findings in this study, the harvester of interest is generalized as a base-excited bistable system having either electromagnetic or piezoelectric conversion mechanisms, the latter components of which are connected to an external resistor (Figure 1), which is a conventional representation of a generic electrical load. The governing equations for the coupled system are expressed as

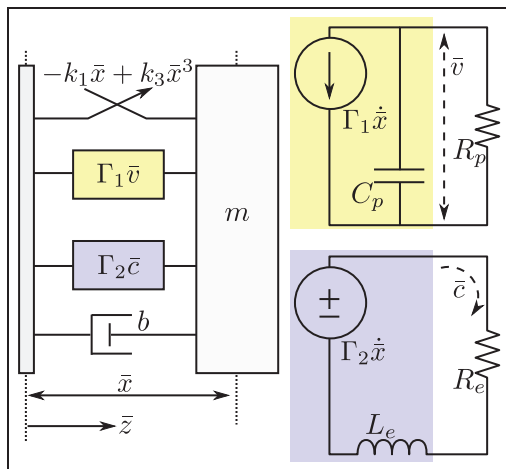


Figure 1. Bistable energy harvester driven by base excitation having either piezoelectric or electromagnetic conversion mechanisms, and corresponding harvesting circuits.

$$m\ddot{x} + b\dot{x} - k_1\bar{x} + k_3\bar{x}^3 = -m\ddot{z} - \Gamma_1\dot{v} - \Gamma_2\dot{c} \quad (2)$$

$$C_p\dot{v} + \frac{1}{R_p}v = \Gamma_1\dot{x} \quad (3)$$

$$L_e\dot{c} + R_e c = \Gamma_2\dot{x} \quad (4)$$

where \bar{z} is the base motion given by $\ddot{\bar{z}} = -P_o \cos \Omega\tau$; \bar{x} is the bistable harvester displacement; \bar{v} is the voltage across the load resistance R_p ; \bar{c} is the current flow through resistance R_e ; m is the mass; b is the mechanical damping constant; k_1 and k_3 are linear and nonlinear stiffness terms, respectively; C_p is the piezoelectric capacitance; L_e is the electromagnetic converter inductance; Γ_1 and Γ_2 are piezoelectric and electromagnetic coupling constants, respectively; and the overdot is differentiation with respect to time τ . Following nondimensionalization and simplification, the governing equations may be reduced to satisfy either harvester configuration

$$x'' + \gamma x' - x + \beta x^3 = p \cos \omega t - \epsilon \theta i \quad (5)$$

$$i' + \rho i = \theta x' \quad (6)$$

The following parameters are defined

$$t = \omega_o\tau; \omega = \Omega/\omega_o; \omega_o = \sqrt{k_1/m}; \gamma = b/m\omega_o; \beta = k_3x_o^2/m\omega_o^2; p = P_o/x_o\omega_o^2 \quad (7)$$

$$i = v; \epsilon = \frac{C_p}{m} \left(\frac{v_o}{x_o\omega} \right)^2; \theta = \frac{x_o\Gamma_1}{v_o C_p}; \rho = \frac{1}{R_p C_p \omega_o}; \quad \text{for piezoelectric coupling} \quad (8)$$

$$i = c; \epsilon = \frac{L_e}{m} \left(\frac{c_o}{x_o\omega} \right)^2; \theta = \frac{x_o\Gamma_2}{v_o L_e}; \rho = \frac{R_e}{L_e\omega_o}; \quad \text{for electromagnetic coupling} \quad (9)$$

where x_o , v_o , and c_o are characteristic length, voltage, and current, respectively, such that $x = \bar{x}/x_o$, $v = \bar{v}/v_o$, and $c = \bar{c}/c_o$. Here, (') indicates differentiation with respect to nondimensional time t . We note that formulation of equations (5) to (9) extends the technique earlier employed where focus was directed to electromagnetic induction harvester designs (Mann et al., 2012). In equations (5) to (9), the term ρ represents the ratio of electrical to mechanical natural frequencies, θ is analogous to a “transducer constant,” and ϵ is an electromechanical coupling term.

Solutions to equations (5) and (6) are assumed in the form of Fourier series expansions

$$x(t) = c + a_1 \sin \omega t + b_1 \cos \omega t + a_3 \sin 3\omega t + b_3 \cos 3\omega t \quad (10)$$

$$i(t) = g_1 \sin \omega t + h_1 \cos \omega t + g_3 \sin 3\omega t + h_3 \cos 3\omega t \quad (11)$$

where the coefficients slowly vary in time. The constant term, c , is required to describe the bistable device

dynamics since the oscillator permits low-energy orbits around one of the stable equilibrium positions.

Amplitude response equations

Equations (10) and (11) are substituted into equations (5) and (6) and the coefficients of the constant, $\sin\omega t$, $\cos\omega t$, $\sin 3\omega t$, and $\cos 3\omega t$ terms are equated

$$-\gamma c' = \Lambda_c c \quad (12)$$

$$-\gamma a'_1 + 2\omega b'_1 = \Lambda_1 a_1 - \omega \gamma b_1 + \frac{3}{4}\beta(-a_1^2 + b_1^2)a_3 - \frac{3}{2}\beta(a_1 b_1)b_3 + \epsilon \theta g_1 \quad (13)$$

$$-2\omega a'_1 - \gamma b'_1 = \omega \gamma a_1 + \Lambda_1 b_1 + \frac{3}{2}\beta(a_1 b_1)a_3 + \frac{3}{4}\beta(-a_1^2 + b_1^2)b_3 + \epsilon \theta h_1 - p \quad (14)$$

$$-\gamma a'_3 + 6\omega b'_3 = \frac{1}{4}\beta(-a_1^2 + 3b_1^2)a_1 + \Lambda_3 a_3 - 3\omega \gamma b_3 + \epsilon \theta g_3 \quad (15)$$

$$-6\omega a'_3 - \gamma b'_3 = \frac{1}{4}\beta(-3a_1^2 + b_1^2)b_1 + 3\omega \gamma a_3 + \Lambda_3 b_3 + \epsilon \theta h_3 \quad (16)$$

$$\theta a'_1 - g'_1 = \omega \theta b_1 + \rho g_1 - \omega h_1 \quad (17)$$

$$\theta b'_1 - h'_1 = -\omega \theta a_1 + \omega g_1 + \rho h_1 \quad (18)$$

$$\theta a'_3 - g'_3 = 3\omega \theta b_3 + \rho g_3 - 3\omega h_3 \quad (19)$$

$$\theta b'_3 - h'_3 = -3\omega \theta a_3 + 3\omega g_3 + \rho h_3 \quad (20)$$

where the following terms are defined

$$\Lambda_c = -1 + \beta \left(c^2 + \frac{3}{2}r_1^2 + \frac{3}{2}r_3^2 \right) \quad (21)$$

$$\Lambda_1 = -1 - \omega^2 + \beta \left(3c^2 + \frac{3}{4}r_1^2 + \frac{3}{2}r_3^2 \right) \quad (22)$$

$$\Lambda_3 = -1 - 9\omega^2 + \beta \left(3c^2 + \frac{3}{4}r_3^2 + \frac{3}{2}r_1^2 \right) \quad (23)$$

$$r_1^2 = a_1^2 + b_1^2 \quad (24)$$

$$r_3^2 = a_3^2 + b_3^2 \quad (25)$$

Steady-state dynamics are predicted in the event that the time derivatives are zero. Using this assumption, the electrical expression coefficients are solved directly from equations (17) to (20) in terms of the mechanical coefficients

$$g_1 = \omega \Phi_1 a_1 - \rho \Phi_1 b_1 \quad (26)$$

$$h_1 = \rho \Phi_1 a_1 + \omega \Phi_1 b_1 \quad (27)$$

$$g_3 = 3\omega \Phi_3 a_3 - \rho \Phi_3 b_3 \quad (28)$$

$$h_3 = \rho \Phi_3 a_3 + 3\omega \Phi_3 b_3 \quad (29)$$

$$f_1^2 = g_1^2 + h_1^2 \quad (30)$$

$$f_3^2 = g_3^2 + h_3^2 \quad (31)$$

$$\Phi_1 = \frac{\omega \theta}{\rho^2 + \omega^2} \quad (32)$$

$$\Phi_3 = \frac{3\omega \theta}{\rho^2 + 9\omega^2} \quad (33)$$

Equations (30) and (31) provide the electrical response amplitudes associated with the fundamental and third harmonics, respectively. Equations (26) to (29) are then substituted into equations (15) and (16) to solve for coefficients a_3 and b_3

$$a_3 = -\frac{1}{4\Delta_3}\beta((\Lambda_3 + 3\epsilon\theta\Phi_3\omega)(-a_1^2 + 3b_1^2)a_1 + (3\gamma\omega + \epsilon\theta\Phi_3\rho)(-3a_1^2 + b_1^2)b_1) \quad (34)$$

$$b_3 = \frac{1}{4\Delta_3}\beta((3\gamma\omega + \epsilon\theta\Phi_3\rho)(-a_1^2 + 3b_1^2)a_1 - (\Lambda_3 + 3\epsilon\theta\Phi_3\omega)(-3a_1^2 + b_1^2)b_1) \quad (35)$$

$$\Delta_3 = (\Lambda_3 + 3\epsilon\theta\Phi_3\omega)^2 + (3\gamma\omega + \epsilon\theta\Phi_3\rho)^2 \quad (36)$$

Finally, equations (26), (27), (34) and (35) are substituted into equations (13) and (14). The resulting equations are squared and summed to obtain the first frequency response equation (37).

$$256\Delta_3 p^2 = (9\beta^4 r_1^8 + 96\Sigma\beta^2 r_1^4 + 256\Delta_1\Delta_3)r_1^2 = \kappa r_1^2 \quad (37)$$

$$\Delta_1 = (\Lambda_1 + \epsilon\theta\Phi_1\omega)^2 + (\gamma\omega + \epsilon\theta\Phi_1\rho)^2 \quad (38)$$

$$\Sigma = (\gamma\omega + \epsilon\theta\Phi_1\rho)(3\gamma\omega + \epsilon\theta\Phi_3\rho) - (\Lambda_1 + \epsilon\theta\Phi_1\omega)(\Lambda_3 + 3\epsilon\theta\Phi_3\omega) \quad (39)$$

Unlike the one-term solution formulations (Mann et al., 2012; Stanton et al., 2012b), the frequency response equation (37) contains two unknowns to be computed: the two nondimensional response amplitudes r_1 and r_3 . Thus, a second equation is required. This is determined by squaring and summing equations (34) and (35).

$$16\Delta_3 r_3^2 = \beta^2 r_1^6 \quad (40)$$

The harmonic balance frequency response equations using the superharmonic terms in the expansion produce two coupled, nonlinear equations (37) and (40) which must be solved for r_1^2 and r_3^2 , after which the electrical response amplitudes, equations (30) and (31), may be computed. Average nondimensional electrical power is computed by equations (41) and (42) for power proportional to the fundamental and third harmonics, respectively

$$P_1 = \frac{1}{2}\rho f_1^2 = \frac{1}{2}\rho\Phi_1^2(\rho^2 + \omega^2)r_1^2 = \frac{1}{2}\rho\frac{\omega^2\theta^2}{\rho^2 + \omega^2}r_1^2 \quad (41)$$

$$P_3 = \frac{1}{2}\rho f_3^2 = \frac{1}{2}\rho\Phi_3^2(\rho^2 + 9\omega^2)r_3^2 = \frac{1}{2}\rho\frac{9\omega^2\theta^2}{\rho^2 + 9\omega^2}r_3^2 \quad (42)$$

Finally, for completeness, the final two coefficients are presented explicitly.

$$a_1 = \frac{16}{\kappa}p(3\beta^2(3\gamma\omega + \epsilon\theta\Phi_3\rho)r_1^4 + 16\Delta_3(\gamma\omega + \epsilon\theta\Phi_1\rho)) \quad (43)$$

$$b_1 = \frac{16}{\kappa}p(-3\beta^2(\Lambda_3 + 3\epsilon\theta\Phi_3\omega)r_1^4 + 16\Delta_3(\Lambda_1 + \epsilon\theta\Phi_1\omega)) \quad (44)$$

Thus, having solved equations (37) and (40) for the nondimensional response amplitudes r_1 and r_3 and corresponding powers P_1 and P_3 , the coefficients may be computed from equations (26) to (29); (34) and (35); and (43) and (44), and stability could be resolved via a perturbation approach around the fixed point (Nayfeh and Balachandran, 1995). The following study focuses on interwell responses for which $c^2 = 0$. However, if low-energy orbit solutions are also desired, c^2 may be determined from steady-state consideration of equation (12) and these results may be substituted into the routine given above for corresponding intrawell response predictions.

Procedure for equation solving

The present Fourier series expansion yields two nonlinearly coupled polynomials, equations (37) and (40), the solutions (i.e. roots) to which thereafter determine the harvester responses. The authors therefore utilize the MATLAB command *fsolve* which has been widely employed in recent vibrations research along with similar computational techniques (Cha and Chen, 2010; DeSmidt, 2010; Moghimi Zand et al., 2009; Padmanabhan and Singh, 1995; Sracic et al., 2012). For the present interest in steady-state interwell responses, the benefits of the proposed model formulation and solution method over alternative numerical solutions, for example, continuation methods, are the substantially reduced computational effort and confidence of an analytically derived result.

Analytical study system parameter selection

Throughout the following studies, parameters employed in analyses are identical to those utilized earlier (Mann et al., 2012): $\gamma = 0.01$, $\beta = 0.09$, $\theta = 10$, $\rho = 2500$, and $\epsilon = 0.8$. Damping γ is set to a value comparable to a harvester exhibiting mild, hysteretic material losses. The selection of β , as a ratio of nonlinear to linear restoring forces in the double-well

potential, can be realistically varied over a wide range based on design parameters such as axial load on a clamped-clamped beam (Masana and Daqaq, 2012) or repulsive magnet distance (Stanton et al., 2010). The electrical and electromechanical parameters θ , ρ , and ϵ are characteristic of inertial generators having very high electrical natural frequency with respect to mechanical resonance and a mild degree of coupling, which is common for many electromagnetic harvester realizations (Mann and Sims, 2010); typical piezoelectric harvester designs may exhibit smaller natural frequency ratios ρ but comparable-order coupling terms θ and ϵ (Liao and Sodano, 2009). In the following, our primary focus is on the influence of *excitation level* upon inducement of superharmonic effects in key frequency bands; this is justified because an individual bistable energy harvester placed in an ambient environment is likely to be exposed to a large range of excitation levels while system design parameters remain mostly constant. However, it may be shown from use of the proposed model and solution method that many of the same results hereafter discovered have comparable (but not identical) trends when changing other parameters such as damping γ or nonlinearity strength β .

Comparison against one-term harmonic balance solution

The importance of considering the additional superharmonic response within the harmonic balance analysis is compared against the one-term solution formulation earlier presented in the literature (Mann et al., 2012; Stanton et al., 2012b). Figure 2(a) and (b) presents the results of one- and two-term harmonic balance solutions for mechanical response amplitudes and electrical power, respectively, for excitation level $p = 0.2$ which represents a mild excitation level for bistable oscillators according to the normalization scheme. In light of the experimental results in this research, further remarks on excitation level classification will be provided later for more intuitive interpretation. Up to $\omega \approx 0.15$, several stable high-energy orbit solutions are predicted using the two-term harmonic balance. As excitation frequency approaches $\omega \rightarrow 0.3$, the two-term superharmonic power begins to increase dramatically above the term related to the fundamental harmonic, a feature observed over a large range of excitation amplitudes by Masana and Daqaq (2012) and explicitly predicted by the present analysis. This effect is indicated in the expression for superharmonic power, equation (42), since the superharmonic power term is multiplied by a factor including $9\omega^2$ as opposed to ω^2 for the fundamental harmonic, equation (41). The most important reason explaining why the superharmonic power does not always exceed the fundamental harmonic component in Figure 2 is that the superharmonic mechanical

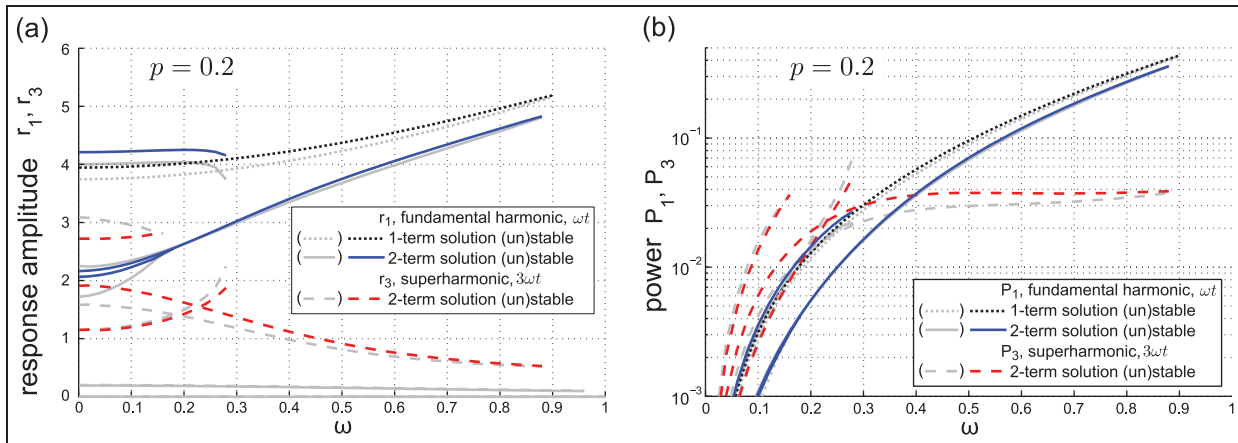


Figure 2. Comparison of one- and two-term solutions for $p = 0.2$ for ωt (fundamental harmonic) and $3\omega t$ (superharmonic). Frequency dependence of (a) response displacement amplitudes and (b) harvested power.

response is shown to substantially decrease for $\omega \gtrsim 0.3$. (Admittedly, the denominator of equation (42) also increases slightly faster than that of equation (41) for $\omega > 1$, but both denominators include term $\rho^2 = 2500^2$ which dwarfs the influence of the other denominator terms in this respect.)

Although the one- and two-term solutions are in fair agreement at frequencies less than $\omega \approx 0.3$ in terms of the fundamental harmonic response amplitude trend, near $\omega \approx 0.3$ the fundamental response computed with a two-term formulation decreases significantly onto another stable solution branch in consequence to a response-annihilating saddle-node bifurcation. This feature was explicitly observed in experiments and correspondingly shown in numerical integration simulations (and only using base acceleration of 2.0 m/s^2) (Masana and Daqaq, 2012) but not yet predicted analytically. After the decrease in response amplitude, Figure 2 shows that the subsequent stable response amplitude gradually follows similar trends as the one-term solution when ω increases. The harvested power similarly grows following the bifurcation at $\omega \approx 0.3$. This comparison shows that even for relatively small excitation levels, the one-term harmonic balance solution is incapable of providing complete insight into the refined dynamics and resulting harvested power induced by the superharmonic response, several characteristics of which were observed in past simulations and experiments (Masana and Daqaq, 2012) and will be further validated and explored in this study. It should be emphasized that comparison between one- and two-term solutions is best made in terms of general response trends and predicted phenomena instead of quantitative response amplitude values; in other words, because the two-term formulation “balances” more of the spectral energy, the two-term net response amplitude $|x| = (r_1^2 + r_3^2)^{1/2}$ will be distinct from the one-term response amplitude $|x| = r_1$. This explains why the

specific amplitudes in Figure 2 differ between the two solution formulations and encourages comparison based on response trends and phenomena.

Finally, it is observed that both one- and two-term harmonic balance solutions predict stable responses extending to asymptotic values as $\omega \rightarrow 0$. These responses are not necessarily stable and realizable but are the consequence of odd-order Fourier series solution expansion. It has been shown that even-order expansions enable determination of criteria for symmetry breaking bifurcation which denotes the realizable lower frequency limit of response existence (Szemplińska-Stupnicka and Rudowski, 1993). Thus, to determine boundaries which demarcate realizable interwell responses from the more likely intrawell oscillations in this low-frequency regime, either the prior method may be employed or more exhaustive basin of attraction numerical studies may be conducted. Furthermore, some of the responses in Figure 2(a) have individual amplitudes less than the distance between a stable equilibria position x^* and the central unstable position: $r_{1,3} < x^* = 1/\sqrt{\beta} = 3.3\bar{3}$. This may lead one to believe that the system is not genuinely snapping through. However, the net response amplitude is the vector sum of r_1 and r_3 : $|x| = (r_1^2 + r_3^2)^{1/2}$. In Figure 2(a), for some combination of responses $r_{1,3}$ the vector sum is always greater than x^* ; however, it will be found in studies hereafter using different excitation levels that the net response amplitude may in fact be less than that of the stable equilibria position, $|x| < x^*$, which has important energy harvesting implications to be discussed.

Effects of increasing excitation amplitude

Excitation amplitude $p = 1.6$

Previous research has shown that manifestation of superharmonic response is amplified as a result of

increasing excitation amplitude (Masana and Daqaq, 2012; Nayfeh and Mook, 1995; Szemplińska-Stupnicka, 1968). Since the excitation amplitude term p is normalized to the linear stiffness of the bistable device which may be very small (Masana and Daqaq, 2012), it is therefore plausible that a bistable harvester will regularly encounter “high” excitation levels. Furthermore, the above comparison against the one-term harmonic balance analysis showed that substantial deviation in responses was predicted when incorporating superharmonic contribution even for mild excitation levels. This makes critical an evaluation of the associated induced superharmonic response and other dynamic effects over a broader range of excitation amplitudes above the mild levels thus far considered and continued validation by numerical simulation and experiments.

Figure 3 plots system responses for excitation level $p = 1.6$. For clarity, this amplitude will be referred to as “moderate,” those lower as “low” or “mild” levels, and those greater as “high” levels. All other system parameters remain the same as in the prior section. Interwell response amplitudes $r_{1,3}$ computed from long-time, direct simulation of governing equations (5) and (6) are given as data points in Figure 3(a); for each excitation frequency ω , the data points are the fundamental ω and superharmonic 3ω spectral components from a fast Fourier transform of the numerically integrated steady-state response x , which is identical in form to the presentation provided by the two-term harmonic balance. As evidenced in Figure 3, inclusion of the superharmonic terms in the analysis results in refined electrodynamic features in the range of $0.15 < \omega < 0.3$. At $\omega \approx 0.15$, a superharmonic response appears due to saddle-node bifurcation, producing a sudden increase in electrical power. As the frequency is increased toward $\omega \approx 0.3$, the superharmonic power continues to increase until a second saddle-node bifurcation eliminates its dominance. This effect simultaneously induces a sudden decrease in the system response for the fundamental term, mechanically and electrically. Increasing

the frequency still further, the fundamental harmonic mechanical response and electrical power become dominant. As shown in Figure 3(a), numerical simulations follow the predicted response trends, notably verifying the importance of the superharmonic spectral contribution and response-altering phenomena in the bandwidth around $\omega \approx 0.3$. It is noted that simulations were unable to locate the response pair in Figure 3(a) predicted at frequencies $\omega < 0.3$ where the fundamental and superharmonic components have comparable response amplitude, indicating their existence is practically marginalized, as least for the present system parameters.

For excitation frequency, $\omega > 0.3$, the electrical power attributed to the superharmonic component continues to increase, despite the fact that the superharmonic displacement amplitude asymptotically approaches a constant value. This is due to the feature mentioned in the prior section regarding the superharmonic power multiplicative factor $9\omega^2$. However, the substantial reduction in the corresponding superharmonic response amplitude r_3 at higher frequencies explains why the power component P_3 never exceeds power proportional to the fundamental response P_1 . There also appears a coexistent stable but low-magnitude interwell response at frequencies greater than $\omega \approx 0.3$. This is an intriguing dynamic feature which will be further considered in the next section.

To provide greater clarity to the appearance of the superharmonic responses, Figure 4 presents the results of forcing $p = 1.6$ but focused specifically onto the superharmonic bandwidth. Within the bandwidth near $0.07 \lesssim \omega \lesssim 0.3$, a bifurcation is predicted to induce a response pair characterized by fundamental and superharmonic response spectra having comparable amplitudes ranging $1.5 \lesssim r_{1,3} \lesssim 3.5$, which could also be observed in coarser resolution via Figure 3. However, numerical simulations did not detect their existence after numerous runs but instead repeatedly located the response pair characterized by much greater fundamental response, although the numerically evaluated

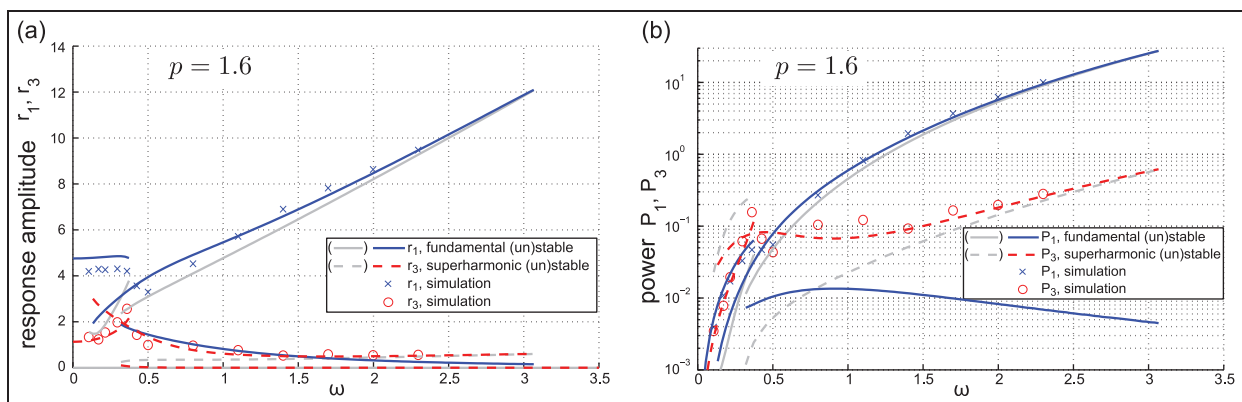


Figure 3. Frequency dependence of (a) response amplitude and (b) average harvested power for $p = 1.6$.

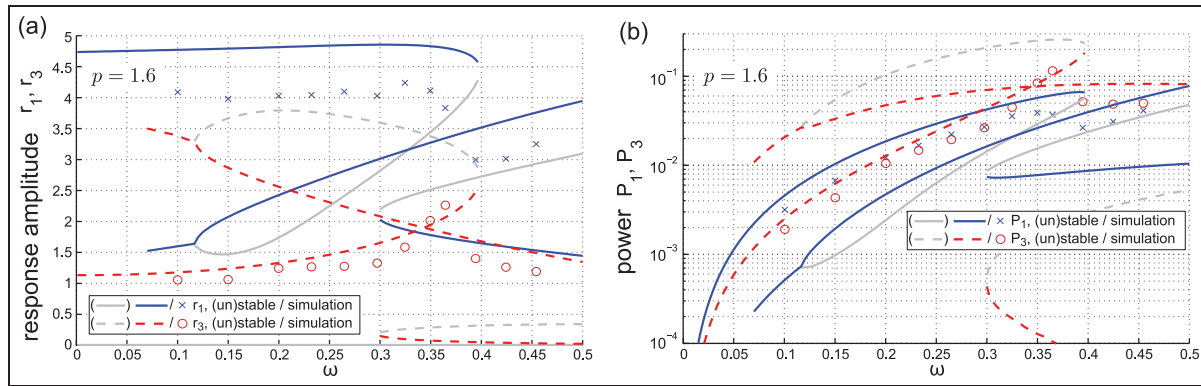


Figure 4. Frequency dependence of (a) response amplitude and (b) average harvested power for $p=1.6$. Focus on superharmonic frequency bandwidth.

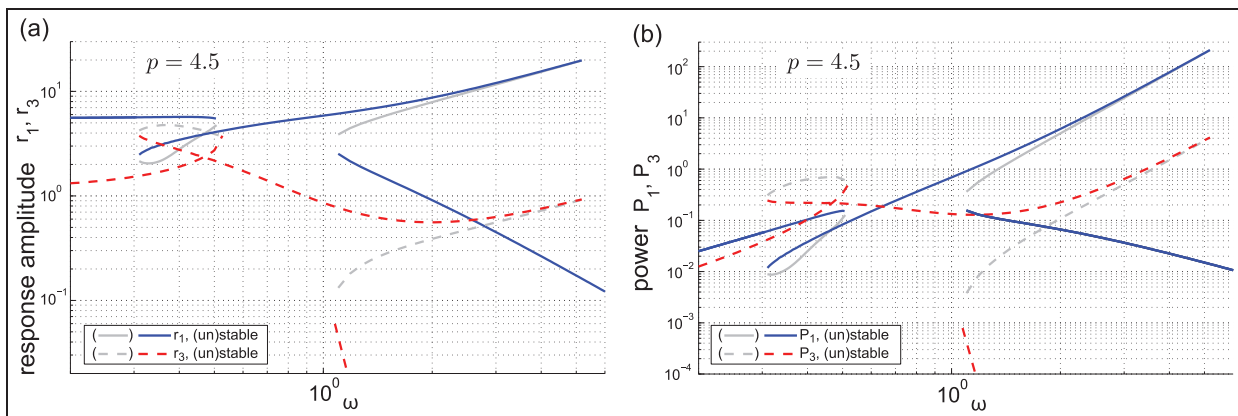


Figure 5. Frequency dependence of (a) response amplitude and (b) average harvested power for $p = 4.5$.

fundamental response of this latter solution pair was determined to be closer to $r_1 \approx 4$ than the predicted $r_1 \approx 4.5$. Near $\omega \approx 0.4$, the system is predicted to plainly undergo a saddle-node bifurcation of the two existent stable responses at which point the new trajectories decrease significantly in amplitude and follow the prior unrealized response branches. Simulations likewise observe this dramatic event, although it occurs closer to normalized excitation frequency $\omega = 0.36$. The sudden decrease in fundamental mechanical response (about 20%–25% reduction) shown in Figure 4(a) was earlier observed to a similar degree (Masana and Daqaq, 2012). The inclusion of superharmonic dynamics to the harmonic balance analysis is capable of predicting these dynamic features, and therefore more accurately reflects the experimentally and numerically observed bistable energy harvesting phenomena in this bandwidth.

Excitation amplitude $p = 4.5$

Figure 5 plots the predicted responses for an excitation amplitude of $p = 4.5$; other system parameters remain the same from prior studies. To more easily observe all

the features, the plots are provided in logarithmic scale. As was shown for the case of $p = 1.6$, a number of bifurcations appear in the superharmonic regime which substantially increase harvested power and ultimately cause the high-energy orbit of the fundamental harmonic to decrease in amplitude near $\omega \approx 0.5$. While the specific superharmonic response of bistable energy-harvesting devices is one focus of this work, the overall dynamic response due to a large range of excitation levels is of equal interest as this was not considered by earlier investigations and we have thus far observed that superharmonic correction in the analyses has not been trivial even for low excitation amplitude (see Figure 2).

Past harmonic balance analyses using one-term expansions indicated a number of regimes in which low-energy and high-energy orbits of the fundamental harmonic were alternatively activated depending on frequency and excitation level (Mann et al., 2012; Stanton et al., 2012b). From these studies it was shown that for very low excitation levels, only low-energy orbits are possible; for intermediate excitation levels, low-energy and high-energy orbits are coexistent depending on initial conditions; for greater excitation levels, only high-energy orbits were predicted.

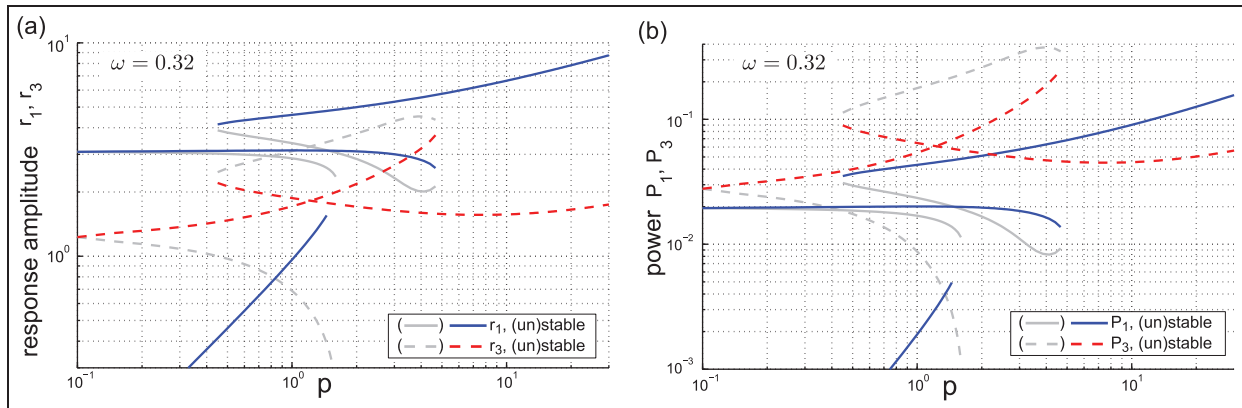


Figure 6. Excitation amplitude dependence of (a) response amplitude and (b) harvested power. $\omega = 0.32$.

Then considering Figure 5 once more, it is interesting to observe the additional stable interwell response predicted to first exist as a consequence of bifurcation at $\omega \approx 1$. The corresponding superharmonic component is of insignificant amplitude and only its initial branching point near $\omega \approx 1$ is shown in Figure 5. The net response amplitude for this response pair is less than the vibration magnitude between the two wells, $|x| = \sqrt{r_1^2 + r_3^2} < 1/\sqrt{\beta} = 3.3\bar{3}$, which diminishes further as excitation frequency increases. The phase of this response lags the excitation by approximately 180° , where phase lag of the fundamental harmonic ϕ_1 is computed from $\tan(\phi_1) = a_1/b_1$ (not plotted here for brevity). Given that the dynamic represents an interwell oscillation in the sense that the response mean is zero over a forcing period (i.e. the model employing $c^2 = 0$ predicts its existence), this indicates that the unstable central equilibrium position of the harvester becomes stabilized in consequence to the high level and frequency of excitation. In other words, the system undergoes exceptionally small oscillations, comparable to an intrawell response, but instead of oscillating about a *stable* equilibria, the bistable harvester exhibits zero-mean interwell harmonic response around the central *unstable* equilibrium such that $|x| < 1/\sqrt{\beta}$. This phenomenon is known as excitation-induced stability (EIS), is a consequence of parametric-type excitation, and is recognized as one means of stabilizing systems such as inverted pendula (Ibrahim, 2006). When perturbed around an interwell response solution, the bistable oscillator governing equation takes the form of a Mathieu–Hill equation (Tseng and Dugundji, 1971) which represents a parametrically excited system; this gives further evidence that the phenomena observed in Figure 5 for stable, very low response amplitude—but still *interwell*—vibrations is indicative of EIS.

Therefore, depending on the excitation frequency and amplitude, there may be coexistent interwell responses representing a high-energy snap-through dynamic favorable for energy harvesting and an

adverse cross-well response characterized by near stationarity of the harvester inertial mass. The likelihood of attaining each response (including potential coexisting intrawell orbits) is subject to initial condition sensitivity and may be characterized by evaluating the basins of attraction (Wiggins, 2003). However, the lack of reports of EIS for bistable energy harvesters in the literature, and the authors’ own numerical and experimental investigations which did not give evidence of such behaviors, may indicate the EIS phenomenon has low degree of realization for practical bistable harvester configurations.

Just as proper bistable energy harvester design is necessary to initially attain high-energy orbits and therefore maximize electrical power, we find that it is equally important to know the range of excitation level and frequency that may provide undesirable opportunity for the breakdown of the high-energy orbits. These are global features of energy harvesting using bistable devices which had not been classified with the earlier analyses but appear more plainly in the present investigation in considering a broad range of excitation inputs.

Superharmonic energy harvesting analysis

Following consideration of the frequency bandwidths over which power proportional to superharmonic spectral components may be superior to that obtained via the fundamental response, the investigations now seek to determine the excitation level regime over which superharmonic power is in fact superior. Since the superharmonic response of this study occurs primarily around $\omega \approx 0.3$, it is logical to focus on frequencies in this range. Figure 6 presents the dependence of bistable harvester responses on excitation amplitude p while excitation frequency remains fixed $\omega = 0.32$. All other system parameters remain the same as in the prior studies. Even for very low excitation amplitude in this key frequency range $\omega \approx 0.3$, the superharmonic response is found to yield a greater level of harvested power than

that component related to the fundamental harmonic. This was observed in Figure 2(b) in initially comparing the one- and two-term solutions. Thus, the superharmonic harmonic balance analysis shows that superior power harvesting may be achieved in this bandwidth which is an important insight the one-term solution is inherently incapable of predicting. Thus, the *net* harvested power increases in this bandwidth but the primary cause is due to the third harmonic 3ω response as compared to the spectral component proportional to the driving frequency ω .

The advantage of superharmonic power harvesting is even greater when the excitation level is increased so as to induce saddle-node bifurcation near $p \approx 0.4$. From approximately $0.45 < p < 4.5$, the superharmonic power is noticeably greater than the component proportional to the fundamental harmonic response, as much as four times greater (Figure 6(b)). Interestingly, however, above this excitation amplitude both fundamental and superharmonic responses undergo another saddle-node bifurcation which reduces the magnitude of superharmonic mechanical response. As a result, the maximum power output is reduced to the level achievable by the fundamental harmonic. This shows that superharmonic energy harvesting is not necessarily superior even in the frequency range where the effect is dominant should the excitation amplitude exceed a critical value: for the present parameters, approximately $p = 4.5$. Once again, this implies that a careful understanding of the excitation frequency and amplitude for a given bistable energy harvester is important so as to attain maximum superharmonic energy harvesting performance, in the same way that the fundamental harmonic response need also be considered.

Experimental investigation

In addition to the agreement of the above analytical results to the numerical findings and to the previously published experimental and direct simulation results (Masana and Daqaq, 2012), this section presents new experimental validation and evidence of the ready inducement of superharmonics for bistable energy harvesters. A clamped, ferromagnetic spring steel beam buckled via magnetic attraction is employed (Figure 7). The beam has length $L = 134$ mm, width 12.7 mm, and thickness 0.508 mm. The magnets are stood off from the free beam tip by $\delta = 6$ mm with their centers equidistant to the beam tip equilibrium position when the magnets are absent: $d = 14$ mm. In this configuration, the two intrawell natural frequencies (and damping ratios) were measured to be 14.94 Hz (0.016) and 15.06 Hz (0.019) with stable equilibria at $\bar{x} \pm 5.06$ mm, ensuring as close to ideal symmetry of the double-well potential was achieved. Piezoelectric polyvinylidene fluoride (PVDF) patches of 28 μm thickness are

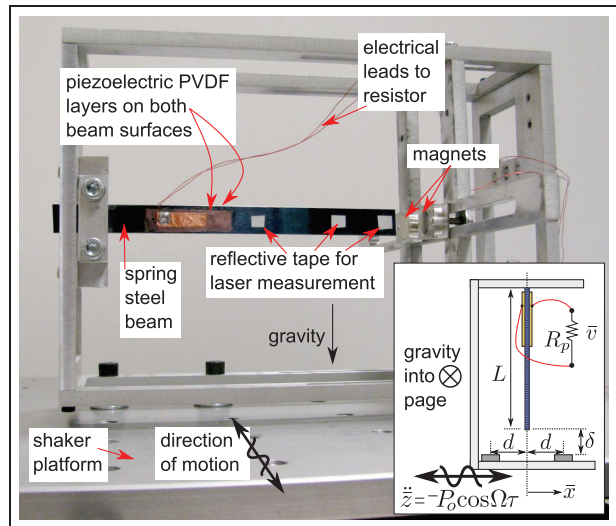


Figure 7. Experimental setup. Postbuckled ferromagnetic beam with piezoelectric PVDF patches, attached to shaker platform, with PVDF electrode leads connected to external resistance (not shown).

applied to both beam surfaces near the clamped end with poled axes facing outward and electrode leads connected in series to an external load resistance $R_p = 4.5$ M Ω . The frame to which the beam was clamped is firmly attached to an electrodynamic shaker in an orientation such that gravitational influences do not affect beam response in the axis of motion. The measured responses during testing are the base acceleration, beam tip velocity and displacement, and the voltage across the load resistor.

A series of experiments is conducted to evaluate the dependence on increasing excitation level to consistently induce prominent superharmonic spectral response in the bandwidth near normalized excitation frequency $\omega \approx 0.3$ and to validate the existence of key stable responses. For each test, the shaker base acceleration level is fixed while very slow increasing frequency sweeps of harmonic base motion are conducted, + 0.01 Hz/s, to ensure quasi-stationary excitations over a given period of time. After data are acquired, autospectral density of the beam velocity is calculated over time intervals spanning 4 s, and thus 0.04 Hz of slow sweep elapsed during this period. The spectral lines of commensurate frequency with the excitation ω and that of three times the drive 3ω are extracted from calculated autospectra and are plotted in the left column of Figure 8. The corresponding horizontal axis data point therefore represents the mean instantaneous normalized excitation frequency which occurs during the 4-s interval of sweeping. In the left column of autospectral velocity responses, only interwell responses are plotted, including chaos; the absence of data points indicates the harvester beam response was confined to intrawell oscillations. The right column shows the

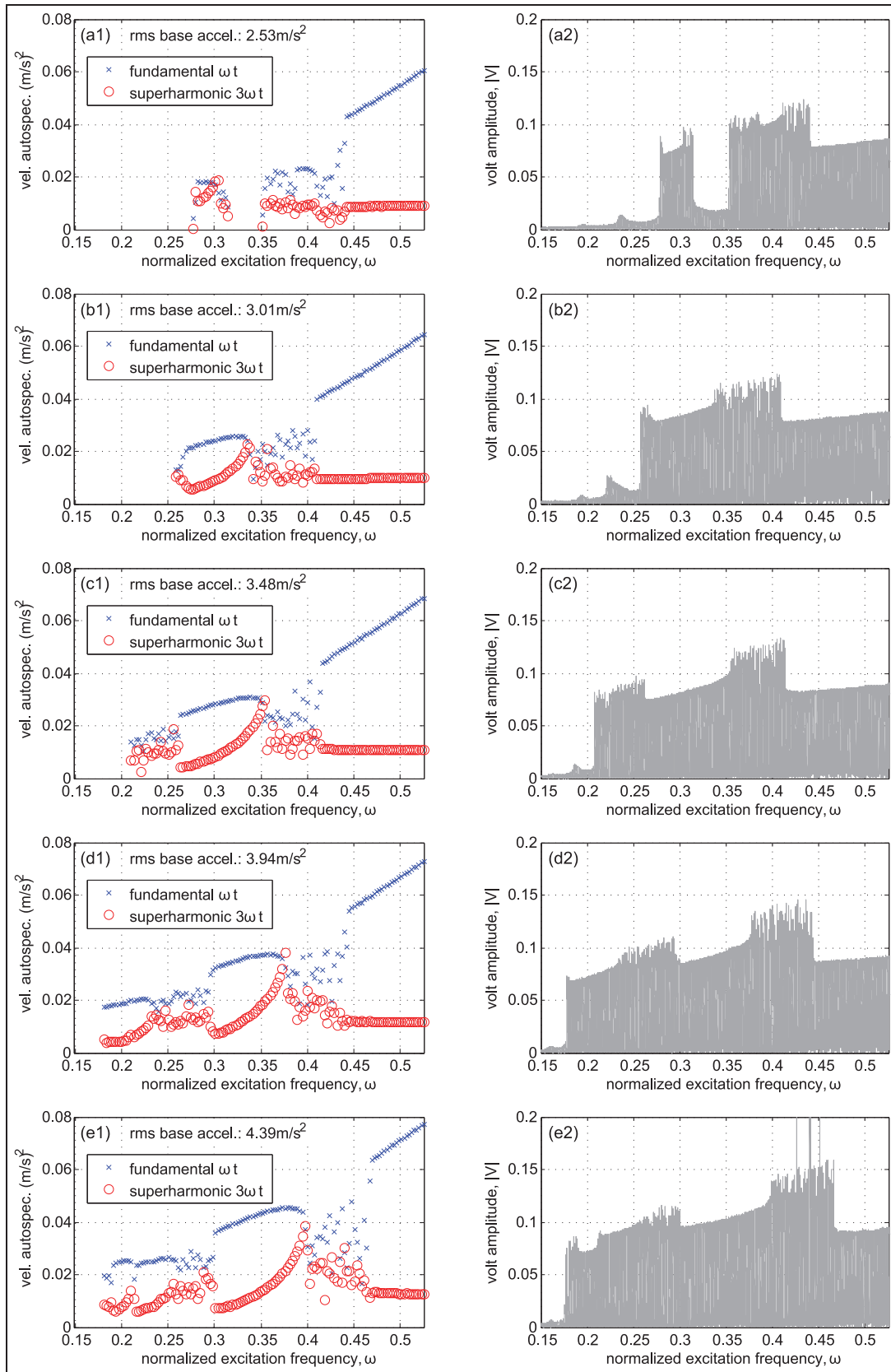


Figure 8. Experimentally measured bistable harvester responses. Left column (1), beam tip interwell velocity autospectral density components of fundamental ω and superharmonic 3ω in consequence to excitation at given ω . Right column (2), piezoelectric voltage amplitude during slow excitation frequency sweep. (a) EL = 2.53 m/s², (b) EL = 3.01 m/s², (c) EL = 3.48 m/s², (d) EL = 3.94 m/s² and (e) EL = 4.39 m/s². EL: excitation level.

complete sweeping time series of the piezoelectric voltage amplitude.

As excitation (base acceleration) level increases, top to bottom in Figure 8, the existence of stable responses in the key bandwidth near $\omega = 0.3$ correspondingly increases. In every case, the existence of these responses is destabilized during the sweep once fundamental and superharmonic spectral components are almost equal, thereafter the periodic responses undergo a decrease in level due to a return to intrawell or chaotic dynamics. The frequency at which the annihilation of response occurs is unique with respect to the excitation level but typically occurs in the range $0.3 \lesssim \omega \lesssim 0.4$. These findings are in excellent agreement with trends observed in Figures 2 to 5, and particularly as analytically predicted and numerically demonstrated in Figure 4(a), where saddle-node bifurcation phenomena are shown to destabilize the fundamental and superharmonic responses. Experimentally, it is seen that the lower response trajectories after the bifurcation event are chaotic (more so evident in the right column of Figure 8), persisting until approximately $0.4 \lesssim \omega \lesssim 0.45$ at which point interwell responses are recaptured and the bistable harvester undergoes the advantageous primarily pure-harmonic snap-through dynamic. For frequencies higher than the point at which the interwell responses are restabilized $\omega \gtrsim 0.45$, the superharmonic 3ω component is of negligible amplitude as compared to the fundamental, but the 3ω harmonic in fact contributes the highest proportion of any additional spectral line as excitation frequency continues to increase (full sweeping spectra not shown for conciseness). This is also in good agreement with analyses which indicated that following the bifurcation near the superharmonic bandwidth $\omega \approx 0.3$, the fundamental response would dominate the overall harvester response. The experimental results plainly indicate which of the response branches predicted by analyses are the stable fundamental–superharmonic response pair in the regime prior to the bifurcation, $\omega \lesssim 0.4$; the existent pair constitutes the large amplitude fundamental ω and the smaller amplitude superharmonic 3ω which exhibit an asymptotic-like approach in magnitudes (ω component decreasing and 3ω component increasing) just prior to destabilization, prominently observed in the left column of Figure 8. After the bifurcation phenomena and decrease in net system response, the new trajectories (i.e. spectral components) follow response profiles comparable to those predicted by analysis and numerical simulation in Figures 3 and 4 in the range $0.35 \lesssim \omega \lesssim 0.4$. However, experimentally, prior to obtaining the smooth fundamental and superharmonic responses, the system undergoes chaotic vibrations until the frequency sweep reaches approximately $0.4 \lesssim \omega \lesssim 0.45$.

Figure 9(a) plots the measured voltage autospectral components of the fundamental and superharmonic

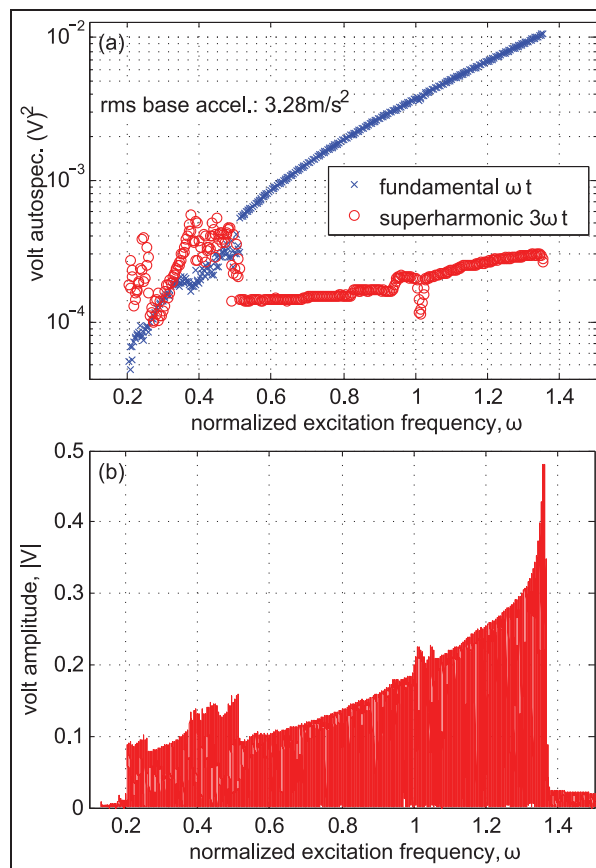


Figure 9. Experimentally measured bistable harvester piezoelectric voltages. (a) Autospectral density components of interwell fundamental ω and superharmonic 3ω voltages in consequence to excitation at given ω . (b) Voltage amplitude. Excitation level = 3.28m/s^2 .

spectral lines for a full frequency sweep lasting from the initial onset of interwell dynamics near $\omega \approx 0.2$ up to the normalized excitation frequency at which the pure-harmonic snap-through response destabilizes and the harvester returns to intrawell dynamics, $\omega \approx 1.37$. The corresponding voltage amplitude sweeping time series is given in Figure 9(b). Note that the average generated power is proportional to the squared voltage amplitude spectral components by way of the load resistance and coupling terms; thus, a plot of average power on a logarithmic scale would be proportional by a constant factor to Figure 9 and extend the orders of magnitude spanned such that all the salient trends of the voltage plot of Figure 9(a) have comparable relation to power plots of the analyses. The potentially misleading nature of plotting “average power” for measured responses which undergo chaos is justification for plotting voltage instead of power; in contrast, for analyses where chaotic responses are not predicted by steady-state investigations, this difficulty of presentation is not encountered and thus plots of power were provided. For base acceleration of 3.28m/s^2 , the first responses to be activated

are chaotic, persisting until onset of the dramatic superharmonic effects observed near $\omega \approx 0.25$. The multi-harmonic responses remain stable up to bifurcation near $\omega \approx 0.35$ after which the system returns to a chaotic response. Around the bandwidth $0.3 \lesssim \omega \lesssim 0.4$ in Figure 9(a), however, it is found that the voltage response proportional to the superharmonic 3ω becomes substantially amplified with respect to the fundamental ω (as much as 3.2 times at $\omega = 0.377$), which verifies the analytical predictions throughout this work that superharmonic electrical responses in this bandwidth may become notably superior to the fundamental harmonic responses. Following the recapturing of snap-through response near $\omega \approx 0.5$, the superharmonic voltage spectrum continues to increase as frequency increases but not to the same degree exhibited by the fundamental term. Overall, these trends are in good agreement with the predictions for normalized excitation level $p = 1.6$ (Figure 3), although the system was estimated to sustain interwell response to higher normalized excitation frequency. This latter deviation may be due to the extremely slow rate of frequency sweeping because it is known that optimized sweep rates are necessary to probe the full frequency extent of stable, nonlinear responses (Nayfeh and Mook, 1995).

In light of the comparable results between experiments and analysis, it appears that one way to determine approximate translation between the arbitrary low–moderate–high excitation level classification used in the analytical studies and the known experimental base acceleration levels is to observe the frequency at which the destabilizing superharmonic bifurcation event occurs. In analysis, it was observed that this frequency increased from $\omega \approx 0.3$ at $p = 0.2$ (low/mild excitation level) to approximately $\omega \approx 0.4$ for $p = 4.5$ (high excitation level). Likewise, in Figure 8, it is found that the destabilization event occurs at $\omega \approx 0.3$ for base acceleration of 2.53 m/s^2 and at $\omega \approx 0.4$ for acceleration of 4.39 m/s^2 . Thus, for the present system, the “low” to “high” classification used in the analytical studies appears to also characterize the full range of excitation levels evaluated in the laboratory. This is by no means a comprehensive excitation level ranking system, but is described to highlight the fairly narrow excitation level range across which the present experimental bistable harvester transitioned from relatively mild- to high-level regimes, requiring adjustment of base acceleration level from 2.53 m/s^2 to only 4.39 m/s^2 . While one example of many potential bistable energy harvester systems and configurations, these findings indicate the relative ease with which dramatic superharmonic effects may become highly activated, leading to important superharmonic 3ω spectral concentration (near $\omega \approx 0.3$) and diffusion (during continuous snap through) of the response and electrical energies.

Conclusion

A model for a bistable energy-harvesting device is presented and its electrodynamic equations solved using the method of harmonic balance having fundamental and superharmonic components. Model investigations explicitly predict a host of new dynamical features which have been observed in prior experimental and direct numerical simulation studies but not yet captured analytically. Due to the nature of bistable devices having relatively low linear stiffness (or linear natural frequency) which serves as the normalization parameter for excitation level, even a mild level of excitation may induce significant superharmonic effects, a trend consistently observed in the present analyses and experimental studies.

Harvested power related to the superharmonic response is predicted to be greater than that related to the fundamental harmonic response in a certain bandwidth, up to a critical excitation amplitude. Experimental results provide validation to the numerous trends predicted by analyses and give strong evidence of the ease at which superharmonic spectral diffusion may occur with bistable systems. However, this finding is not disadvantageous because harvested power proportional to the third harmonic was shown by analysis, numerical simulation, and experiment to potentially increase significantly above power proportional to the fundamental harmonic in the band of frequencies near $\omega \approx 0.3$. With these insights, it can be concluded that substantial deviation between predicted and true system responses may occur if employing insufficient models without consideration of superharmonic dynamics. Overall, the results of this research indicate that effective bistable energy harvesting design and implementation requires a clear understanding of the input excitation characteristics relative to the device design parameters so as to appropriately harness the superharmonic effects.

Declaration of conflicting interests

The authors declared no potential conflicts of interest with respect to the research, authorship, and/or publication of this article.

Funding

This research received no specific grant from any funding agency in the public, commercial, or not-for-profit sectors.

References

- Betts DN, Kim HA, Bowen CR, et al. (2012) Optimal configurations of bistable piezo-composites for energy harvesting. *Applied Physics Letters* 100: 114104.
- Cha PD and Chen CY (2010) Quenching vibration along a harmonically excited linear structure using lumped masses. *Journal of Vibration and Control* 17(4): 527–539.
- Daqaq MF (2011) Transduction of a bistable inductive generator driven by white and exponentially correlated Gaussian noise. *Journal of Sound and Vibration* 330: 2554–2564.

- Daqaq MF (2012) On intentional introduction of stiffness nonlinearities for energy harvesting under white Gaussian excitations. *Nonlinear Dynamics* 69: 1063–1079.
- DeSmidt HA (2010) Analysis of a dual gearbox/shaft system with nonlinear dynamic mesh phase interactions. In: *Proceedings of the 51st AIAA/ASME/ASCE/AHS/ASC structures, structural dynamics and materials conference*, Orlando, FL, 12–15 April, AIAA-2010-2893.
- Erturk A, Hoffmann J and Inman DJ (2009) A piezomagnetoelastic structure for broadband vibration energy harvesting. *Applied Physics Letters* 94: 254102.
- Falnes J (2002) *Ocean Waves and Oscillating Systems: Linear Interactions Including Wave-Energy Extraction*. Cambridge: Cambridge University Press.
- Feeny BF and Yuan CM (2001) Parametric identification of an experimental magneto-elastic oscillator. *Journal of Sound and Vibration* 247: 785–806.
- Ferrari M, Ferrari V, Guizzetti M, et al. (2010) Improved energy harvesting from wideband vibrations by nonlinear piezoelectric converters. *Sensors and Actuators A* 162: 425–431.
- Harne RL and Wang KW (2013) A review of the recent research on vibration energy harvesting via bistable systems. *Smart Materials and Structures* 22: 023001.
- Harne RL, Thota M and Wang KW (2013) Concise and high-fidelity predictive criteria for maximizing performance and robustness of bistable energy harvesters. *Applied Physics Letters* 102: 053903.
- Ibrahim RA (2006) Excitation-induced stability and phase transition: a review. *Journal of Vibration and Control* 12(10): 1093–1170.
- Karami MA and Inman DJ (2011) Equivalent damping and frequency change for linear and nonlinear hybrid vibrational energy harvesting systems. *Journal of Sound and Vibration* 330: 5583–5597.
- Kim GW and Kim J (2013) Compliant bistable mechanism for low frequency vibration energy harvester inspired by auditory hair bundle structures. *Smart Materials and Structures* 22: 014005.
- Liao Y and Sodano HA (2009) Structural effects and energy conversion efficiency of power harvesting. *Journal of Intelligent Material Systems and Structures* 20: 505–514.
- Malatkar P and Nayfeh AH (2007) Steady-state dynamics of a linear structure weakly coupled to an essentially nonlinear oscillator. *Nonlinear Dynamics* 47: 167–179.
- Mann BP and Owens BA (2010) Investigations of a nonlinear energy harvester with a bistable potential well. *Journal of Sound and Vibration* 329: 1215–1226.
- Mann BP and Sims ND (2010) On the performance and resonant frequency of electromagnetic induction energy harvesters. *Journal of Sound and Vibration* 329: 1348–1361.
- Mann BP, Barton DAW and Owens BAM (2012) Uncertainty in performance for linear and nonlinear energy harvesting strategies. *Journal of Intelligent Material Systems and Structures* 23: 1451–1460.
- Masana R and Daqaq MF (2011) Relative performance of a vibratory energy harvester in mono- and bi-stable potentials. *Journal of Sound and Vibration* 330: 6036–6052.
- Masana R and Daqaq MF (2012) Energy harvesting in the super-harmonic frequency region of a twin-well oscillator. *Journal of Applied Physics* 111: 044501.
- Moghimi Zand M, Ahmadian MT and Rashidian B (2009) Semi-analytic solutions to nonlinear vibrations of microbeams under suddenly applied voltages. *Journal of Sound and Vibration* 325: 382–396.
- Nayfeh AH and Balachandran B (1995) *Applied Nonlinear Dynamics: Analytical, Computational, and Experimental Methods*. Weinheim: Wiley.
- Nayfeh AH and Mook DT (1995) *Nonlinear Oscillations*. Weinheim: Wiley.
- Padmanabhan C and Singh R (1995) Analysis of periodically excited non-linear systems by a parametric continuation technique. *Journal of Sound and Vibration* 184: 35–58.
- Rao HVSG (1984) Research in vibration analysis of highway bridges. *Shock and Vibration Digest* 16: 17–22.
- Sracic MW, Yang S and Allen MS (2012) Comparing measured and computed nonlinear frequency responses to calibrate nonlinear system models. In: Adams D, Kerschen G and Carrella A (eds) *Topics in Nonlinear Dynamics, Volume 3: Proceedings of the 30th IMAC, A Conference on Structural Dynamics 2012*. New York: Springer, pp. 255–267.
- Stanton SC, Mann BP and Owens BAM (2012a) Melnikov theoretic methods for characterizing the dynamics of a bistable piezoelectric inertial generator in complex spectral environments. *Physica D* 241: 711–720.
- Stanton SC, McGehee CC and Mann BP (2010) Nonlinear dynamics for broadband energy harvesting: investigation of a bistable piezoelectric inertial generator. *Physica D* 239: 640–653.
- Stanton SC, Owens BAM and Mann BP (2012b) Harmonic balance analysis of the bistable piezoelectric inertial generator. *Journal of Sound and Vibration* 331: 3617–3627.
- Stephen NG (2006) On energy harvesting from ambient vibration. *Journal of Sound and Vibration* 293: 409–425.
- Szemplińska-Stupnicka W (1968) Higher harmonic oscillations in heteronomous non-linear systems with one degree of freedom. *International Journal of Non-Linear Mechanics* 3: 17–30.
- Szemplińska-Stupnicka W and Rudowski J (1993) Steady states in the twin-well potential oscillator: computer simulations and approximate analytical studies. *Chaos* 3: 375–385.
- Tang L, Yang Y and Soh CK (2010) Toward broadband vibration-based energy harvesting. *Journal of Intelligent Material Systems and Structures* 21: 1867–1897.
- Tseng WY and Dugundji J (1971) Nonlinear vibrations of a buckled beam under harmonic excitation. *Journal of Applied Mechanics* 38(2): 467–476.
- Tweten DJ and Mann BP (2013) On the use of weighting matrices to improve harmonic balance parameter identification results. *Journal of Sound and Vibration* 332: 2941–2953.
- Wiggins S (2003) *Introduction to Applied Nonlinear Dynamical Systems and Chaos*. New York: Springer.
- Williams CB and Yates RB (1996) Analysis of a micro-electric generator for microsystems. *Sensors and Actuators A* 52: 8–11.
- Yuan CM and Feeny BF (1998) Parametric identification of chaotic systems. *Journal of Vibration and Control* 4: 405–426.
- Zhu D, Tudor MJ and Beeby SP (2010) Strategies for increasing the operating frequency range of vibration energy harvesters: a review. *Measurement Science & Technology* 21: 022001.